Available online at www.sciencedirect.com
SCIENCE DIRECT
ELSEVIER
Polymer 46 (2005) 10148–10157
polymer
www.elsevier.com/locate/polymer

Crystallization, melting, and morphology of a poly(ethylene oxide) diblock copolymer containing a tablet-like block of poly{2,5-bis[(4-methoxyphenyl)oxycarbonyl]styrene}

Yun Huang[a], Jing Wang[a], Xuan-Bo Liu[a], Hai-Liang Zhang[a,1], Xiao-Fang Chen[a], Wen-Chang Zhuang[b], Xiao Chen[b], Chun Ye[a], Xin-Hua Wan[a], Er-Qaing Chen[a,*], Qi-Feng Zhou[a,*]

[a]*Department of Polymer Science and Engineering and The Key Laboratory of Polymer Chemistry and Physics of Ministry of Education, College of Chemistry and Molecular Engineering, Peking University, Beijing 100871, China*
[b]*Institute of Colloid and Interface Chemistry, College of Chemistry and Chemical Engineering, Shandong University, Jinan, Shandong 250100, China*

Received 14 April 2005; received in revised form 25 July 2005; accepted 1 August 2005
Available online 25 August 2005

Abstract

A poly(ethylene oxide) diblock copolymer containing a short block of poly{2,5-bis[(4-methoxyphenyl)oxycarbonyl]styrene} (PEO-*b*-PMPCS) has been successfully synthesized via atom transfer radical polymerization (ATRP) method. The number average molecular weights (M_n) of the PEO and PMPCS blocks are 5300 and 2100 g/mol, respectively. Combining the techniques of differential scanning calorimetry (DSC), optical microscopy (OM), wide angle X-ray diffraction (WAXD), and small angle X-ray scattering (SAXS), we have found that the PMPCS blocks, which are tablet-like, can significantly affect the crystallization and melting of the diblock copolymer. The sample studied can form the crystals with a monoclinic crystal structure identical to that of the homo-PEO. The melting temperature (T_m) of the diblock copolymer increases monotonically with crystallization temperature (T_c), which is remarkably similar to the behavior of long period. On the basis of Gibbs–Thomson relationship, the equilibrium T_m (T_m^0) of the diblock copolymer is estimated to be 65.4 °C. In a wide undercooling (ΔT) range (14 °C $< \Delta T <$ 30 °C), the isothermal crystallization leads to square-shaped crystals. The PEO-*b*-PMPCS crystallization exhibits a regime I→II transition at ΔT of 19 °C. The PEO blocks are non-integral folded (NIF) in the crystals, and the PMPCS blocks rejected to lamellar fold surfaces prevent the NIF PEO crystals from transforming to integral folded (IF) ones. Furthermore, the PMPCS tablets may adjust their neighboring positions up or down with respect to the lamellar surface normal, forming more than one PMPCS layer to accompany the increase in the PEO fold length with increasing T_c.

Keywords: Diblock copolymer; Crystallization; Morphology

1. Introduction

In the study of polymer crystallization, low molecular weight (LMW) poly(ethylene oxide) (PEO) fractions have been chosen as a model system for over 30 years [1–3]. One of the most important discovers is that the LMW PEO fractions can form integral folding chain (IF(n), n for the fold number) crystals from melt in the low undercooling (ΔT) range, wherein the lamellar thickness is always fairly an integral fraction of the chain length [4–23]. This fact has been considered to be the direct evidence of chain folding in polymer melt crystallization. Moreover, during the LMW PEO isothermal crystallization, non-integral folding chain (NIF) crystals grow first and subsequently develop into IF crystals via lamellar thickening and/or thinning process [14–23]. Compared with the IF crystals, the NIF crystals are thermodynamically less stable, but possess the most favorable kinetics, i.e. the nucleation barrier of the NIF crystallization is the lowest. The fold length of the initial NIF crystals increases with decreasing ΔT, as commonly observed in polymer lamellar crystals.

* Corresponding authors. Tel.: +86 10 6275 3111; fax: +86 10 6275 3370.
E-mail addresses: eqchen@pku.edu.cn (E.-Q. Chen), qfzhou@pku.edu.cn (Q.-F. Zhou).
[1] Present address: Institute of Polymer Science, Xiangtan University, Xiangtan, Hunan 411105, China.

0032-3861/$ - see front matter © 2005 Elsevier Ltd. All rights reserved.
doi:10.1016/j.polymer.2005.08.010

When the NIF crystals transform into the IF crystals, the LMW PEO chains take sliding diffusion motion along the crystallographic *c*-axis, resulting in the apparent thickening or thinning of lamellar crystals. This molecular diffusion motion is a cooperative one, which may involve two or more chain stems, folds, and chain ends moving simultaneously. Therefore, the NIF→IF crystal transformation exhibits a strong dependence on molecular architecture [19–23]. In particular, upon increasing the end group size of the LMW PEOs, thickening and thinning processes are increasingly hampered [20]. For the LMW PEOs with large end groups, e.g. $-OC(CH_3)_3$ and $-OC_6H_5$, the life time of the NIF crystals can be very long.

While the IF crystals present the most remarkable feature of the final morphologies of the LMW homo-PEO, the crystallization of crystalline–amorphous diblock copolymers containing LMW PEO blocks usually leads to NIF crystals [24–32]. Diblock copolymers may form microphase separation structures [33]. In the strong or medium segregation limit regime away from the order–disorder transition (ODT), the crystallization of PEO blocks will take place within the ordered phase structures. The original ordered phase may be either destroyed if the PEO crystallization temperature (T_c) is higher than the glass transition temperature of amorphous blocks (T_g^a), or otherwise remained, especially when $T_c < (T_g^a)$. In both cases, the crystallization of PEO blocks is in the fashion of chain folding, and the amorphous blocks can be viewed as being tethered on lamellar fold surfaces. The formation of PEO IF crystals is largely prevented, mainly because the amorphous blocks accommodated on lamellar surfaces will be stretched when the tethering density is reduced. Thermodynamically, the final crystal morphology of PEO diblock copolymers reflects the balance between an enthalpic driving force to minimize the fold surface energy and the entropic term from stretching of amorphous blocks [34].

In this publication, we report our study on a PEO diblock copolymer containing a tablet-like short block of poly{2,5-bis[(4-methoxyphenyl)oxycarbonyl]styrene} (PMPCS).

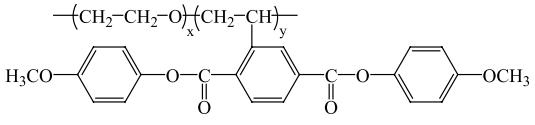

The number average MWs (M_n) of the PEO and PMPCS blocks are 5300 and 2100 g/mol, respectively, corresponding to the degree of polymerizations (DP) $x=120$ and $y=5$. In PMPCS, each mesogenic side group is laterally attached (jacketed) to the polyethylene backbone via a single carbon–carbon bond. Our previous research has showed that PMPCSs with relatively high MW ($M_n \gtrsim 10{,}000$ g/mol, measured by gel permeation chromatography (GPC) using polystyrene (PS) standards for calibration) exhibit columnar liquid crystalline (LC) phases, whereas PMPCSs with $M_n \lesssim 10{,}000$ g/mol are amorphous [35]. The PEO-*b*-PMPCS studied here is therefore a crystalline–amorphous block copolymer. Furthermore, the PMPCS blocks are more or less tablet in shape, which possess the maximum chain length of 1.25 nm (corresponding to five repeating units) and a tablet diameter of approximately 1.7 nm (estimated from wide angle X-ray diffraction (WAXD) results). We expect that such a coil-tablet diblock copolymer will exhibit crystallization behavior different from those observed in either the LMW homo-PEO or the conventional crystalline–amorphous block copolymers. We have investigated the crystal morphologies of the PEO-*b*-PMPCS, trying to understand how the molecules accommodate the PMPCS tablets in amorphous layers when the PEO blocks form folded-chain crystals. The influences of PMPCS blocks on the thermodynamic stability of PEO crystals and the crystallization kinetics are also discussed.

2. Experimental section

2.1. Material synthesis

The PEO-*b*-PMPCS block copolymer was synthesized by atom transfer radical polymerization (ATRP) using a PEO-macroinitiator. The LMW PEO fraction [α,ω-hydroxy-methoxy-poly(ethylene oxide)] (PEO-OH) was purchased from Aldrich. After purification and fractionation, the M_n and polydispersity (dw) of the PEO-OH are 5300 g/mol and 1.03, respectively. Using it as a precursor, a PEO-macroinitiator was prepared according to the method reported by Jankova et al. [36]. The detailed synthetic procedure and characterization of the monomer 2,5-bis[(4-methoxyphenyl)oxycarbonyl]styrene (MPCS) were reported elsewhere [37,38]. To obtain the PEO-*b*-PMPCS diblock copolymer, the MPCS and initiator system (the macroinitiator PEO-Br, CuBr, and Sparteine, with a molar ratio of 1:1:2) were charged into a polymerization tube under ambient atmosphere, followed by adding chlorobenzene. After being degassed with three freeze–thaw cycles, the tube was sealed under vacuum, and immersed into a thermostatted oil bath at a preset temperature of 90 °C. To control the MW of PMPCS to be low, the reaction was ended at a relatively low conversion by quenching the tube into ice–water mixture. The product was diluted with THF, and passed through a neutral alumina column to remove the residual copper complex. The solution was then poured into a large volume of cold methanol under ice water bath to precipitate the resultant diblock copolymer. The precipitation was separated by centrifugation, followed by redissolving in THF and repreciptating in ethyl ether. The final white powder of the diblock copolymer was collected by filtering and dried in vacuum. The M_n of the PMPCS block was measured to be of 2100 g/mol.

2.2. Equipment and experiments

The M_ns of the precursor PEO-OH and the macroinitiator PEO-Br were determined by ^{1}H NMR (Bruker ARX400 spectrometer, $DCCl_3$ as solvent and TMS as internal standard). With the known M_n of PEO block, the copolymer composition and the M_n of PMPCS block were attained by ^{1}H NMR, whereas the MW distribution of the sample was measured by GPC calibrated with PS standard. The chemical structure of the diblock copolymer was determined using ^{1}H MNR and Fourier transfer infrared spectroscopy (FTIR, Magna-IR 750). In addition, the crystalline structure of the PEO-*b*-PMPCS was examined by WAXD experiments performed on a Philips X'pert pro diffractometer with a 3 kW ceramic tube as the X-ray source (Cu Kα) and an X'elerator detector.

Differential scanning calorimetry (DSC, Perkin–Elmer Pyris I) was utilized to study the melting behavior of the PEO-*b*-PMPCS after isothermal crystallization at different T_cs. The temperature and heat flow were calibrated with benzoic acid and indium. The samples were encapsulated in hermetically sealed aluminum pans, with a typical sample weight of approximately 2 mg. Isothermal crystallization was performed by quenching the isotropic melt to the preset T_cs. In the low ΔT range, a self-seeding technique [7] was used to promote the isothermal crystallization process, where samples crystallized at relatively lower T_cs were first heated to a selected self-seeding temperature (T_s) followed by 5–10 min annealing. The samples were directly heated to above melting temperature (T_m) after crystallization. The heating rate dependence of the T_m was studied by varying the heating rate from 1 to 20 °C/min.

The morphologies and linear growth rates of diblock copolymer crystals grown in melt were observed under polarized light microscopy (PLM, Leica DML) in conjunction with a Mettler hot stage (FP-90). A Nomarski differential interference contrast microscope (DIC, Olympus BX51) was also employed to examine the crystal morphologies. The samples were prepared in between two cover glasses with a film thickness of ~0.1 μm. The self-seeding method was used for low ΔTs. The isothermal crystallization was stopped by quickly immersing samples into a dry ice/acetone mixture, leading to tiny crystals overgrown around the crystal perimeters as self-decoration [7]. The long periods of the crystallized samples were determined by small angle X-ray scattering (SAXS), by means of a Kratky compact small-angle system equipped with a position sensitive detector (OED 50M from Mbraun, Graz, Austria) containing 1024 channels with a width of 54 mm. The range of scattering angle was chosen from $s=0.05$ to 6 nm^{-1} (scattering vector $s=2\pi\sin\theta/\lambda$, where 2θ and λ were the scattering angle and an X-ray wavelength of 0.154 nm, respectively). The distance from the sample to detector was 27.7 cm and the exposure time was 3600 s.

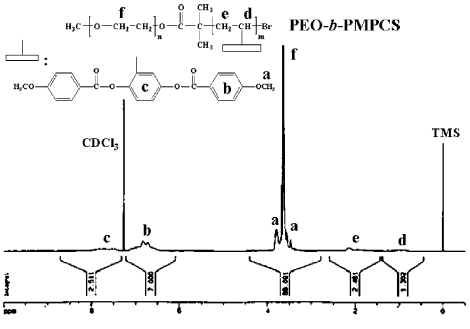

Fig. 1. ^{1}H NMR spectrum of the PEO-*b*-PMPCS.

3. Results

3.1. Molecular and structure analysis

Upon using ATRP, we successfully obtained the PEO-*b*-PMPCS diblock copolymer. The macroinitiator of PEO-Br was found to work effectively for the ATRP of MPCS monomers. After polymerization, the GPC results demonstrated the complete disappearance of PEO-Br, and a unimodal and narrow MW distribution (dw = 1.07) of the copolymer. The ^{1}H NMR spectrum in Fig. 1 shows that the copolymer contains both PEO and PMPCS blocks. On the basis of the spectrum, the weight fraction of the PMPCS block (f_{MPCS}) can be estimated according to:

$$f_{MPCS} = \frac{(I_b M_{MPCS})/8}{(I_b M_{MPCS})/8 + ((I_{a+e} - (6I_b)/8)M_{EO})/4} \quad (1)$$

where M_{MPCS} and M_{EO} are the MWs of the repeating units in PMPCS and PEO, I_b is the integral intensity of hydrogen of the two side benzene rings on the PMPCS side chains, and I_{a+e} is the sum of the integral intensities of the hydrogen of OCH_3 in PMPCS and OCH_2CH_2 in PEO. The f_{MPCS} was calculated to be 28%, corresponding to the PMPCS M_n of 2100 g/mol.

We found that the homo-PMPCS with M_n around 2000 g/mol was amorphous and miscible with LMW PEO above the T_m of PEO. In order to investigate how the short PMPCS blocks affect on the PEO crystalline structure, WAXD experiments were performed after the complete crystallization of the sample. As described in Fig. 2, the WAXD pattern of the PEO-*b*-PMPCS is identical to that of the pure linear PEO with a monoclinic crystal structure [39]. This indicates that the PMPCS blocks are excluded to the amorphous layers between lamellae. On the basis of the WAXD pattern, the crystallinity of the PEO block was estimated to be 77% following a weight correction for the PMPCS block, which was significantly lower than 95% that is usually found for LMW homo-PEO. Also presented in Fig. 2 is the WAXD pattern of homo-PMPCS (M_n = 2300 g/mol) for comparison, of which two amorphous halos are located at 2θ around 5.2 and 20° (d spacings of ~1.7 and ~0.4 nm). However, the low angle amorphous halo of the

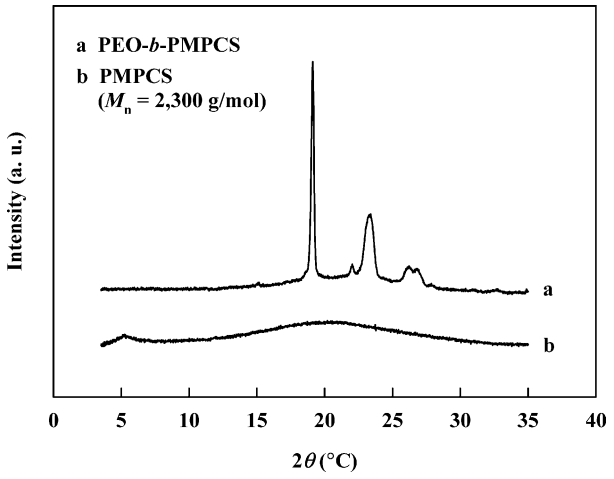

Fig. 2. WAXD patterns of (a) the PEO-*b*-PMPCS after complete crystallization and (b) the PMPCS with M_n of 2300 g/mol.

PMPCS can be detected in neither crystalline nor molten state of the PEO-*b*-PMPCS. The possible reason is that after crystallization, the PMPCS blocks are mixed with the PEO folds and cilia in the amorphous region.

The short PMPCS blocks with only five repeating units are rigid, and more or less tablet-like due to the mesogen jacketing effect. The thickness of the tablet can be simply estimated from the DP of the PMPCS blocks. Given the polyethylene backbones are fully extended, the PMPCS blocks possess a maximum chain length of 1.25 nm, which should be the highest limit of the tablet thickness. On the other hand, the tablet diameter, i.e. the dimension perpendicular to the PMPCS backbones can be deduced from our WAXD result. In our previous research, we have identified that the PMPCS homopolymers with sufficient high MW ($M_n > 1.6\times10^4$ g/mol by GPC) are rod-like, which can closely pack into a hexatic nematic columnar phase [35]. On the basis of the (100) diffraction at 2θ of 6.1°, the rod diameter is calculated to be 1.6 nm. For the amorphous LMW PMPCS, the *d* spacing of 1.7 nm at 2θ around 5.2° (Fig. 2) most likely represents the average distance between the adjacent chain backbones that are jacketed by the mesogen groups. We take this *d* spacing as apparently the diameter of the PMPCS tablets.

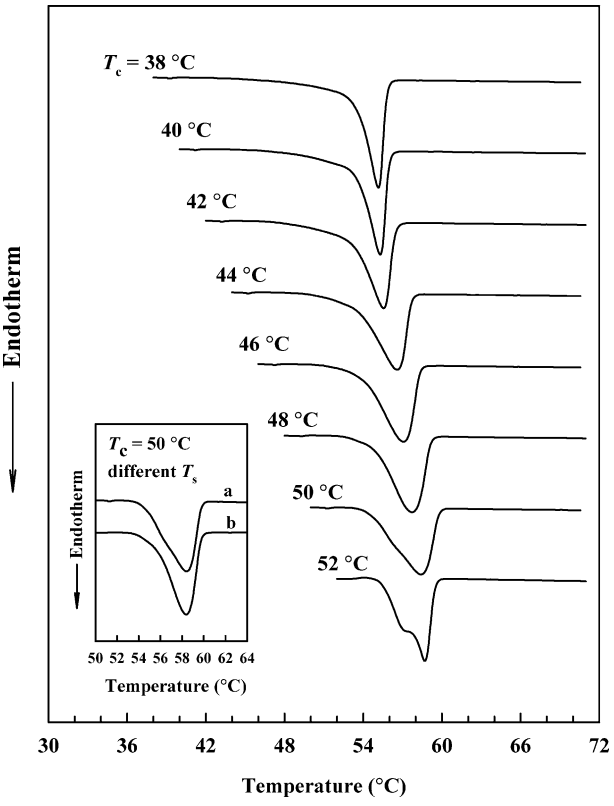

Fig. 3. A set of DSC melting traces obtained at 5 °C/min for the PEO-*b*-PMPCS after isothermal crystallization at different T_cs. The inset shows the melting traces of the sample crystallized at 50 °C with the T_s of 56.5 (a) and 58 °C (b). Curve b of the inset possesses a smaller full width of half height.

3.2. Melting Behavior of PEO-b-PMPCS

The thermal behavior of the PEO-*b*-PMPCS was examined by DSC heating and cooling scans. While the homo-PMPCS with $M_n = 2300$ g/mol exhibits a T_g at 90.0 °C [35], the diblock copolymer only gives the exothermic and endothermic peaks for the PEO crystallization and melting upon cooling and heating, respectively, within a temperature range of −50 to 120 °C. Fig. 3 includes a set of DSC melting traces recorded at 5 °C/min for the copolymer isothermally crystallized at various T_cs. Disregarding the varying of T_c, the heats of fusion (ΔH_f) were always measured to be 103.0 J/g. If using the equilibrium heat of fusion (ΔH_f^0) of 7.89 kJ/mol as the reference for the LMW PEO crystals [12,13], the crystallinity of the sample are 80% after a weight correction for the PMPCS blocks, which is close to the value determined by the WAXD experiments.

When $T_c < 42$ °C, the melting peak temperature (T_p) remains nearly constant at 55.2 °C. When $T_c > 42$ °C, the overall crystallization becomes rather slow. Therefore, the self-seeding method was employed, wherein the crystals formed at 30 °C were first slowly heated to and then annealed 5–10 min at the T_s of 56.5 °C prior to isothermal crystallization. As shown in Fig. 3, the T_p increases monotonically with T_c for $T_c > 42$ °C, accompanying by a peak broadening. At $T_c = 50$ °C, a shoulder starts to develop on the lower temperature side of the melting peak. When further increasing T_c to 52 °C, the higher endotherm with $T_p = 58.5$ °C becomes narrow, and another recognizable peak appears with $T_p = 57.3$ °C. The lower melting peak for the high T_cs (e.g. 50 and 52 °C) was found to be T_s-dependent. For example, using crystals formed at 48 °C as the precursor, we were able to increase the T_s to 58.0 °C. The subsequential isothermal crystallization at 50 °C led to a much narrower melting peak (see the inset of Fig. 3). This implies that at low T_s such as 56.5 °C, while most of the crystals are melted, the survived seeds are difficult to be

fully annealed, and thus, possess a distribution of fold length. In this case, only the seeds with substantially long fold lengths directly induce the growth of lamellae with the thickness determined by the applied ΔT, and the rest seeds with relatively short fold lengths may initially cause the formation of thinner lamellae [40].

After isothermal crystallization of the PEO-*b*-PMPCS at different T_cs, the DSC melting experiments were carried out with different heating rates (Fig. 4). The T_p of the crystals formed at $T_c > 42$ °C increases monotonically with the increasing heating rate, corresponding to a superheating or time lag phenomenon [41]. On the other hand, for $T_c <$ 42 °C, the T_p exhibits an upturn when the heating rate is reduced, which should be associated with annealing or reorganization process [41]. However, as evidenced by the small change in T_p, the original crystals would not change much during slow heating. For example, the crystals formed at 40 °C have a T_p of 55.6 °C at 1 °C/min, only 0.3 °C higher than that at 5 °C/min. Fig. 5 plots the melting temperature (T_m) as a function of T_c. In the plot, the T_ms were estimated by the T_p values that are extrapolated to a heating rate of 0 °C/min (for $T_c < 42$ °C, only the T_p measured at heating rate ≥ 5 °C/min were used). The T_m is nearly constant at 54.9 °C for $T_c < 42$ °C; above this, it increases monotonically and reaches 57.7 °C at $T_c \geq 50$ °C.

3.3. Crystal morphologies and linear growth rates of PEO-*b*-PMPCS

The self-seeding method enables us to control the formation of the PEO-*b*-PMPCS single crystals, of which the morphologies are further visualized by self-decoration. Fig. 6 describes the PLM images of crystals isothermally crystallized at different T_cs. At $T_c \leq 40$ °C, the diblock copolymer forms spherulites with radiating, branched 'fibrous' structures, as evidenced by the irregular Maltese crosses (Fig. 6(a), $T_c = 40$ °C). When 40 °C $< T_c <$ 48 °C, a typical hedritic texture is observed (Fig. 6(b), $T_c = 43$ °C). Further increasing T_c gives the single crystal morphologies such as multilayered lamellae (Fig. 6(c), $T_c = 49$ °C) and single layered lamellae (Fig. 6(d), $T_c = 50$ °C). Interestingly, the spherulites, hedrites, and single crystals of the PEO-*b*-PMPCS are always close to the square shape when $T_c >$ 36 °C. This is significantly different from the usual case of LMW PEO, which exhibits the single crystal morphology with a faceting–rounding–refaceting phenomenon at high T_c and the facet crystals with hexagonal shape.

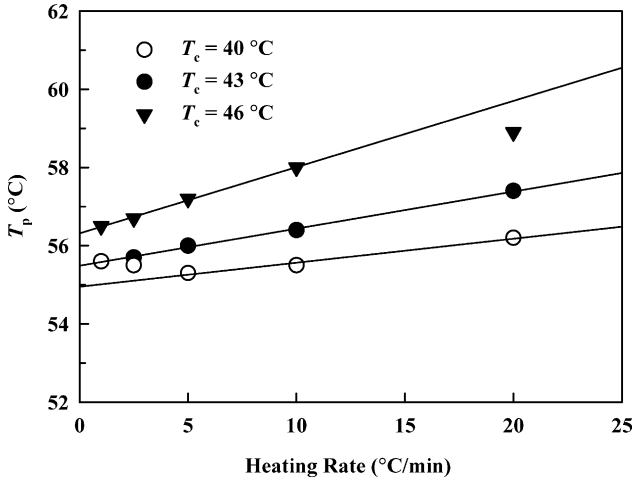

Fig. 4. Melting peak temperature (T_p) vs. heating rate for the sample crystallized at 40, 43, and 46 °C.

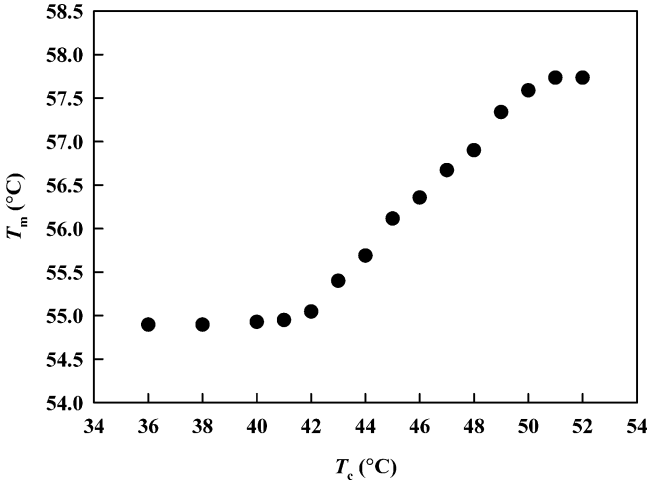

Fig. 5. Relationship between T_m and T_c. The T_ms were estimated by extrapolating the T_p to a heating rate of 0 °C/min.

Fig. 7 shows the DIC images of the crystals formed at 50 °C followed by self-decoration. In Fig. 7(a), the diagonals of the single layer lamella are nearly parallel to the directions of polarizer and analyzer. After deep quenching, two pairs of bright and dark lines are decorated along the lamellar edge. This tells that the lateral surfaces of the single crystals induce the overgrowth of crystals with the PEO chain direction tilted away from the light beam. The width of the decoration lines is ~1 μm, much narrower than that usually found in LMW PEO (~10 μm) using the same self-decoration procedure. Moreover, the lamellar basal surfaces without tiny decorated spherulites look smooth, implying that the possible protrusions or irregularities thereon are not active [7]. In addition to the single layered lamellae, Fig. 7(b) demonstrates a pyramid-like morphology (frequently observed at $T_c = 50$ °C) including four sectors. The 'pyramid' might form due to the spiral growth with screw dislocation as shown in Fig. 7(c). When the terraces are narrow enough, the decoration lines of the adjacent lamellae look merge together, resulting in apparently two pairs of bright and dark sectors and thus, pyramid-like crystals.

On the basis of PLM observation, we measured the size change of the spherulites, hedrites, and single crystals with crystallization time, and thus, the linear growth rates (G) of the diblock copolymer. Fig. 8 presents the plot of logarithmic G vs. T_c. Two crystal growth branches can be

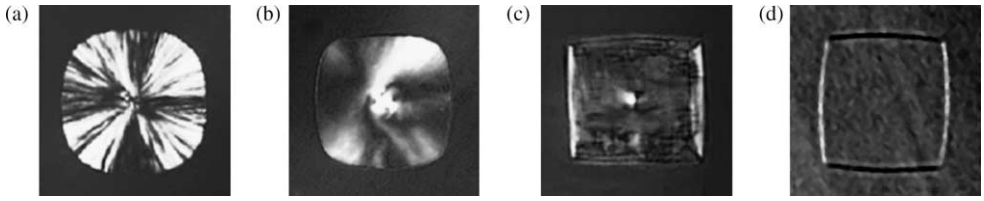

Fig. 6. PLM images of the PEO-*b*-PMPCS crystals formed at (a) 40 °C, (b) 43 °C, (c) 49 °C, and (d) 50 °C.

separated at T_c of 46 °C. In this figure, the crystal growth behavior for the PEO-OH is also provided for comparison. At the same T_c, the G of diblock copolymer is more than one order of magnitude lower than that of the PEO-OH. This reveals that the PMPCS blocks substantially affect the crystallization kinetics of the PEO blocks (see below).

4. Discussion

When conventional crystalline–amorphous diblock copolymers crystallize from melt to form lamellae, the flexible amorphous blocks are tethered on the lamellar fold surfaces. With decreasing ΔT, the lamellar thickness or fold length increases. Accordingly, the area occupied by each amorphous block on fold surfaces continuously decreases, i.e. the tethering density increases, leading to the stretching of the amorphous blocks. However, as described above, the PMPCS blocks are rigid and tablet in shape, with a tablet thickness no more than 1.25 nm and a diameter of ~1.7 nm. We therefore expect the packing behavior of the tablet PMPCS blocks in amorphous layers will be different from that of coil blocks.

The long periods (L) of the PEO-*b*-PMPCS after melt crystallization were measured by SAXS experiments with the results shown in Fig. 9. The L remains 10.5 nm at $T_c \leq 40$ °C, and gradually increases when above this T_c. This behavior of L with T_c is remarkably similar to that of the T_m (Fig. 5). For the lamellar morphology with an assumed two-phase model, the PEO fold length can be calculated by multiplying the L by the volume fraction of the crystallized PEO. With the density of the amorphous layers unknown in our sample, we can only roughly estimate the fold length or lamellar thickness (l_c). Our DSC results reveal that only 80 wt% of PEO blocks are packed into crystalline portion despite the various T_c, i.e. the rest 20 wt% have to stay in amorphous layers and mix with the PMPCS blocks. As a first approximation, we assume that the amorphous volume can be calculated by an addition scheme, using the densities of 1.124 and 1.26 g/cm^3 for the amorphous PEO [41] and PMPCS [35], respectively (the later one was measured by floating technique). Therefore, the volume fraction of the crystallized PEO with a density of 1.239 g/cm^3 [41] is 0.57. The approximate l_c and amorphous layer thicknesses ($l_a = (L - l_c)/2$, the factor of 2 counts the two amorphous layers on top and bottom of a lamella) are also plotted in the inset of Fig. 9 as a function of T_c.

The results in Fig. 9 indicate that the PEO blocks are non-integrally folded in the lamellar crystals. It is known that the PEO chains adopt a 7_2 helical conformation in the monoclinic structure, of which each repeating unit possesses a length of 0.278 nm [39]. For the LMW PEO with $M_n =$ 5300 g/mol, the extended chain length is 33.5 nm. The measured l_cs correspond to the fact that the PEO blocks need to fold four times at $T_c < 46$ °C and three times when $46\ °C \leq T_c \leq 50$ °C. For comparison, we have studied the crystallization and melting of the PEO-OH ($M_n =$ 5300 g/mol), and found that the IF($n > 1$) crystals (and thus

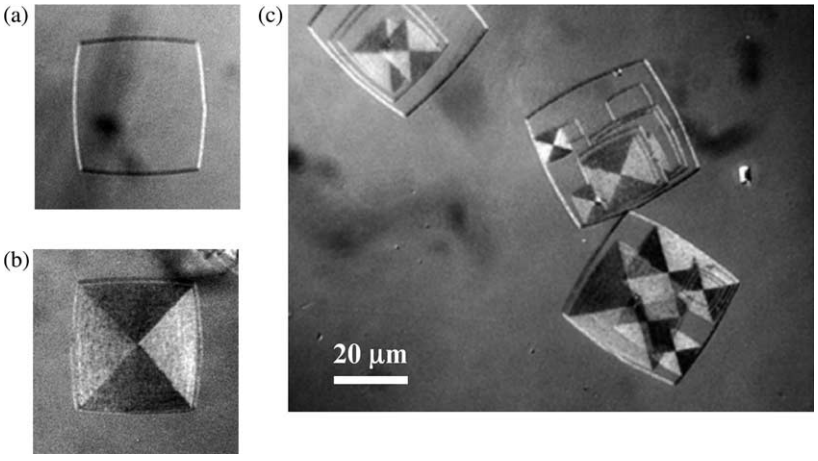

Fig. 7. DIC images of the PEO-*b*-PMPCS crystals formed at 50 °C. The single layered (a) and pyramid-like crystals (b) are observed. The image (c) shows the spiral growth of the crystals.

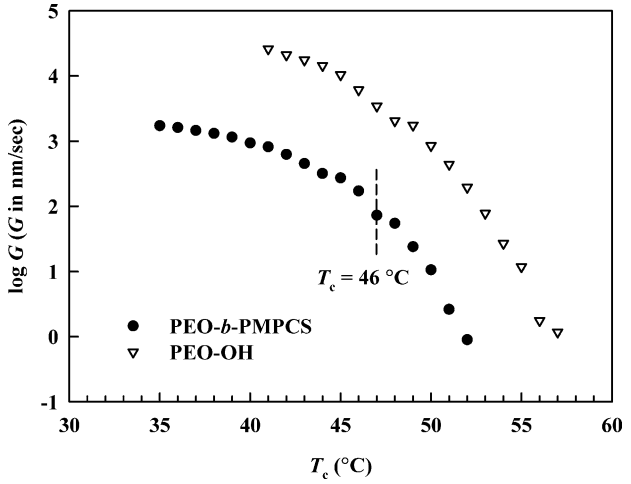

Fig. 8. Linear growth rates (G) of the PEO-*b*-PMPCS and PEO-OH as function of T_c.

$l_c < 16$ nm) of the PEO-OH cannot be detected [13]. The IF($n > 1$) crystals may be unstable and easily transformed into IF($n = 1$) via thickening process. However, the existence of the PEO-*b*-PMPCS crystals with $n > 2$ indicates that the tablet PMPCS blocks prevent the lamellar thickening during and after isothermal crystallization.

After crystallization, the PMPCS blocks should be randomly distributed on both top and bottom fold surfaces with an equal probability. For the PEO-*b*-PMPCS lamellae with the l_a of 2.3–2.5 nm at $T_c \leq 46$ °C, as illustrated in Fig. 10(a), we speculate that the amorphous portion contains one layer of PMPCS tablets. The tablets contribute the thickness of nearly 1.2 nm, and the rest 1.1–1.3 nm of l_a should arise from the 20 wt% of PEO blocks that are not crystallized. The total lamellar surface created by a PEO block with four folds (and thus five stems) in crystal is 2.1 nm^2 [39], while the cross section of the PMPCS tablet with the assumed diameter of 1.7 nm is 2.2 nm^2. This means

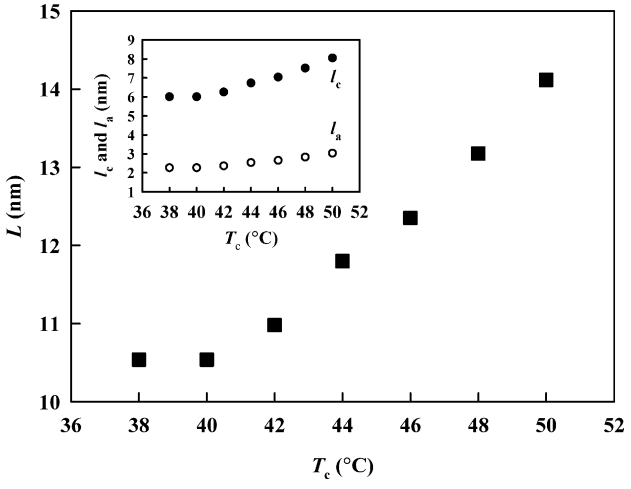

Fig. 9. Relationship between the long period (L) and T_c for the PEO-*b*-PMPCS. The inset shows the calculated lamellar and amorphous layer thicknesses (l_c and l_a) change with T_c.

that when $T_c \leq 46$ °C, the PMPCS blocks are not overcrowded laterally when accommodated within the same layer. Since the rigid PMPCS blocks are unable to pack densely, the PEO cilia and loose folds must also fill the vacancies.

As shown in Fig. 9, the l_c and l_a increase simultaneously with T_c. Since the PMPCS tablets cannot be stretched longer than the ultimate backbone length of 1.25 nm, the increase of l_a must arise from an alternative packing mechanism instead of amorphous block stretching. As the average fold number decreases, the tethering density increases, making the rigid tablets feel overcrowded in a same layer. Consequently, some PMPCS blocks may move ~1 nm away from the surfaces of the crystalline cores, forming a structure with more than a single layer of tablets (Fig. 10(b)). In this case, the upper PMPCS blocks are connected to the crystalline core by the amorphous segments of PEO. For example, when the PEO-*b*-PMPCS crystallizes at 50 °C, the l_a of 3.0 nm can be associated with two layers of PMPCS blocks, wherein each layer is composed of the PMPCS blocks mixing with PEO segments.

The packing model sketched in Fig. 10 may interpret the square-shaped crystal morphologies in Figs. 6 and 7. In the low ΔT range, most of the facet crystals of the LMW homo-PEOs grown from melt are nearly hexagonal, with the folding direction parallel to the (120) planes [42,43]. For star PEOs with two, three, and four LMW PEO arms linked via coupling agents at molecular centers, square-shaped single crystals have been observed [21,44]. It is suggested that the star PEOs may fold along the (100) and (010) planes. Since the distances of adjacent fold sites of (100) and (010) planes are larger than that of (120) planes, folding along these two planes may cost lower energy penalty when the big coupling agents of the star PEOs (~1 nm in lateral dimensions) become part of folds on lamellar surfaces. We consider that the square-shaped crystals of the PEO-*b*-PMPCS develop from a similar packing behavior as in the star PEOs. Although each PEO stem provides same surface area disregarding different fold directions after crystallization, when the PMPCS tablets move to the fold surfaces during crystallization, to minimize the repulsion from each other, the PEO blocks will prefer to folding along (100) and (010) planes. Recently, our selected area electron diffraction on monolayered PEO-*b*-PMPCS crystals grown on carbon surface confirmed that the four edges of the square-shaped crystals are bounded by (100) and (010) planes [45].

Our model may also interpret the formation of pyramid-like crystals. When the copolymer forms more than one layer of PMPCS blocks on fold surfaces at low ΔT, the PEO linkages between the upper PMPCS blocks and the crystalline core will present a length distribution due to inevitable fluctuation. If some sufficiently long PEO linkages are occasionally extended, they may initiate screw dislocation [46]. This process may even start when the lateral size of the basal lamellae is rather small, and

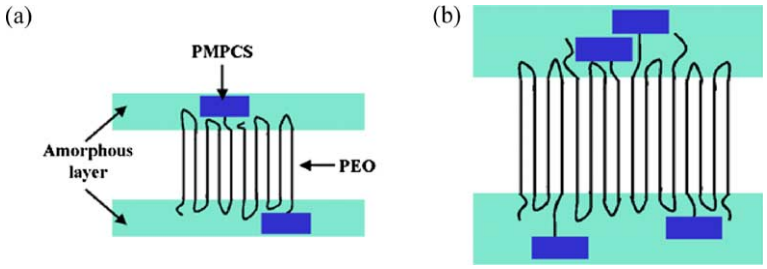

Fig. 10. Schematic representation of the PEO-*b*-PMPCS packing model. At low T_c, the PEO blocks may fold four times and the amorphous part contains one PMPCS layer (a). When the average fold number of PEO blocks decreases to be 3, the amorphous portion may contain two PMPCS layers (b).

continuously take place at crystal growth front, producing a growth spiral. Therefore, under an optical microscope, the multilayered crystals look like to share the same center as a pyramid.

To estimate the equilibrium melting temperature (T_m^0), Fig. 11 illustrates a plot based on Gibbs–Thomson equation, wherein the linear relationship of $T_m \propto 1/l_c$ holds valid for the sample. The T_m^0 of 65.4 °C is found for the PEO-*b*-PMPCS, lower than 68.9 °C of LMW PEO given by Kovacs [12,13]. With the ΔH_f^0 of 7.89 kJ/mol, the calculated σ_e is 21.5 erg/cm^2, which falls within σ_e of 20−30 erg/cm^2 reported for low and moderate MW PEOs [47]. Since a fold surface energy is directly associated with the work of forming the amorphous layer, a higher σ_e is expected for the studied copolymer to further arrange its PMPCS blocks. For that reason, the σ_e of 21.5 erg/cm^2 seems to be underestimated. Furthermore, it is worthy to note that the structure of the amorphous layer changes as the l_a increases with T_c. Strictly speaking, the T_m^0 and σ_e calculated based on Fig. 11 are apparent ones.

Using T_m^0 of 65.4 °C as the reference, we obtained the linear relationship between l_c (also L) and $1/\Delta T$ in Fig. 12. As mentioned above, rather than the fast NIF→IF crystal transformation in LMW PEOs, the PEO-*b*-PMPCS still retains its NIF crystals after isothermal crystallization. Therefore, the l_c should be close to the initial fold length.

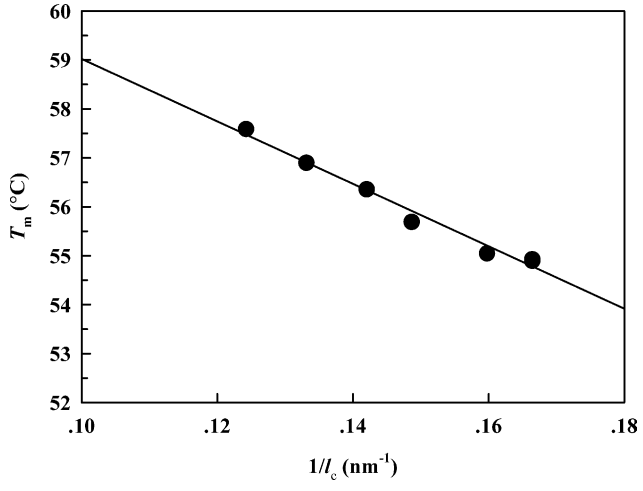

Fig. 11. Relationship between the T_m and reciprocal lamellar thickness (l_c).

The observed $l_c \propto 1/\Delta T$ qualitatively agrees with the nucleation theory of polymer crystallization. On the basis of Hoffman–Lauritzen theory, we further perform the regime analysis by plotting $(\ln G + Q_d^*)/RT_c$ as a function of $1/(T_c\Delta T)$, where G is the linear growth rate, and Q_d^* is the activation energy for reptation and diffusion [48,49]. In such a plot (Fig. 13), the line slope corresponds to a nucleation constant, $K_g = (2jb_0\sigma\sigma_e T_m^0)/(k\Delta H_f^0)$, where j is 2 and 1 for the regime I and II, b_0 is the crystalline molecular thickness in growth direction, and σ is the lateral surface free energy. With the G data in Fig. 8 and Q_d^* of approximately 29.3 kJ/mol [9], the two slopes of the best-fit lines for ΔT below and above 19 °C (T_c of 46 °C) are 4.28 and 7.68 ($\times 10^{-4}$ K^{-2}), respectively. The ratio of them is 1.8, close to the theoretical datum of 2, evidencing a regime I→II transition. When the PEO blocks fold along (100) and/or (010) planes, b_0 is 0.32 nm (an equivalent of the half d spacing of (100) planes). The product of the lateral and folded surface free energy, $\sigma\sigma_e$, can be calculated from the slopes determined, which corresponds to 530 and 591 erg^2/cm^4 for regime I and II. These values are close to the data recently reported for high MW PEO samples and the LMW PEO crystallized from thin film [43,50].

The regime I→II transition is associated with both the single nucleation in regime I and multiple nucleation in regime II on a molecularly flat substrate. In this study, the

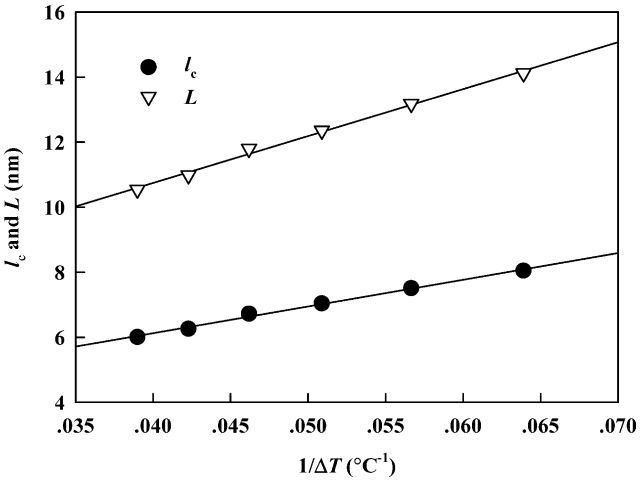

Fig. 12. The lamellar thickness (l_c) and long period (L) as function of the reciprocal undercooling (ΔT).

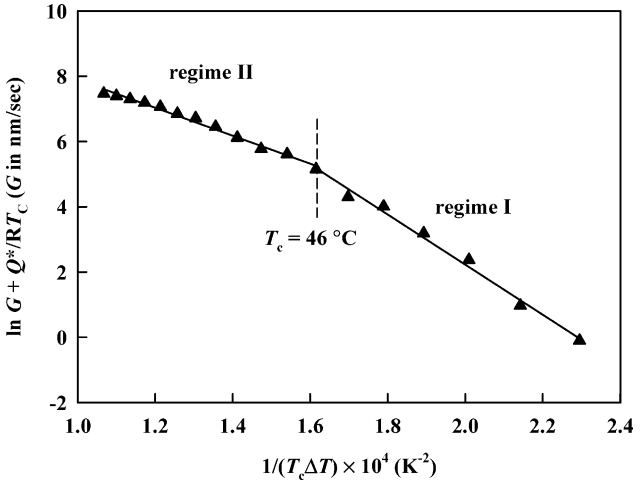

Fig. 13. Plot of $(\ln G+Q^*)/RT_c$ vs. $1/T_c\Delta T$. The regime I→II transition occurs at T_c of 46 °C.

regime transition temperature of $\Delta T = 19$ °C is significantly higher than $\Delta T \sim 10$ °C for the same transition in homo-PEOs with low and moderate MWs [16,47]. This means that the surface nucleation of the PEO-*b*-PMPCS is more difficult. One may imagine that during the crystallization from the isotropic melt, the PMPCS tablets, which are miscible with PEO, can mistakenly attach to the crystal growth front, acting as poisoners. Since the PMPCS tablets are too huge to be tolerated in PEO crystal lattice, the surface nucleation will only occur after they are moved away or rejected towards the fold surfaces. This process will cause an increase in nucleation barrier and retard the crystal growth. Our experimental results show that this poisoning effect is severe, which is obvious in Fig. 8 when one compares the diblock copolymer to its counterpart of PEO-OH. Furthermore, as shown in Figs. 6 and 7, the self-decoration perimeters along the single crystals are much narrower than those usually observed for LMW PEOs. This implies that although the lateral surfaces of the PEO-*b*-PMPCS crystals can provide numerous nucleation sides as LMW PEOs do, its overgrowth during quenching to dry ice/acetone mixture is still subjected to removing the PMPCS blocks from the surface.

5. Conclusion

A diblock copolymer of PEO-*b*-PMPCS, of which the PEO and PMPCS blocks possess the M_n of 5300 and 2100 g/mol, respectively, has been successfully synthesized via ATRP method. The short blocks of PMPCS are rigid and tablet-like. The crystals of the copolymer share the same monoclinic structure as that of homo-PEO, indicating that the PMPCS blocks are rejected to the PEO lamellar surfaces. After isothermal crystallization, the T_m of the sample increases monotonically with T_c, and so it is with the long period. On the basis of Gibbs–Thomson relationship, the T_m^0 of the diblock copolymer is estimated to be 65.4 °C. For $14\ °C < \Delta T < 30\ °C$, the crystals with a square-shaped morphology are observed, indicating that the PEO blocks fold along the (100) and (010) planes. The diblock copolymer crystallizes in a NIF fashion of PEO blocks, of which the fold length is inversely proportional to the ΔT applied. Furthermore, the linear growth rate of the PEO-*b*-PMPCS exhibits a regime I→II transition at ΔT of 19 °C, and the PMPCS blocks can substantially decrease the crystal growth rate. The PMPCS blocks accommodated on the lamellar surfaces prevent the NIF PEO crystals from transforming to the IF ones. When the PEO fold length increases with T_c, the PMPCS blocks may adjust their neighboring positions up or down with respect to the lamellar surface normal, forming the amorphous portion with more than one PMPCS tablet layer.

Acknowledgements

This work was supported by the National Natural Science Foundation of China (Grant no. 20025414, no. 20134010, no. 20234020, and no. 20374003). The authors are grateful to Prof S.Z.D. Cheng, Prof B. Lotz, and Dr F. Khoury for their useful discussions.

References

[1] Buckley CP, Kovcas AJ. In: Hall IH, editor. Structure of crystalline polymers. New York: Elsevier; 1984. p. 261–307.
[2] Cheng SZD, Lotz B. Philos Trans R Soc London, A 2003;361:517.
[3] Reiter G. J Polym Sci, Polym Phys Ed 2003;41:1869.
[4] Arlie JP, Spegt P, Skoulios A. Makromol Chem 1966;99:170.
[5] Arlie JP, Spegt P, Skoulios A. Makromol Chem 1967;104:212.
[6] Spegt P. Makromol Chem 1970;140:167.
[7] Kovacs AJ, Gonthier A. Kolloid ZZ Polym 1972;250:530.
[8] Kovacs AJ, Gonthier A, Straupe C. J Polym Sci, Polym Symp 1975; 50:283.
[9] Kovacs AJ, Straupe C, Gonthier A. J Polym Sci, Polym Symp 1977; 59:31.
[10] Kovacs AJ, Straupe C. Faraday Discuss R Chem Soc 1979;68:225.
[11] Kovacs AJ, Straupe C. J Cryst Growth 1980;48:210.
[12] Buckley CP, Kovacs AJ. Prog Colloid Polym Sci 1975;58:44.
[13] Buckley CP, Kovacs AJ. Colloid Polym Sci 1976;254:695.
[14] Cheng SZD, Zhang AQ, Chen JH, Heberer DP. J Polym Sci, Polym Phys Ed 1991;29:287.
[15] Cheng SZD, Chen JH, Zhang AQ, Heberer DP. J Polym Sci, Polym Phys Ed 1991;29:299.
[16] Cheng SZD, Chen JH. J Polym Sci, Polym Phys Ed 1991;29:311.
[17] Cheng SZD, Zhang AQ, Barley JS, Chen JH, Habenschuss A, Zschack PR. Macromolecules 1991;24:3937.
[18] Cheng SZD, Chen JH, Zhang AQ, Barley JS, Habenschuss A, Zschack PR. Polymer 1992;33:1140.
[19] Cheng SZD, Chen JH, Barley JS, Zhang AQ, Habenschuss A, Zschack PR. Macromolecules 1992;25:1453.
[20] Cheng SZD, Wu SS, Chen JH, Zhou Q, Quirk RP, von Meerwall ED, et al. Macromolecules 1993;26:5105.
[21] Lee SW, Chen EQ, Zhang AQ, Yoon YC, Moon BS, Lee SK, et al. Macromolecules 1996;29:8816.

[22] Chen EQ, Lee SW, Zhang A, Moon BS, Honigfort PS, Mann I, et al. Polymer 1999;40:4543.
[23] Chen EQ, Lee SW, Zhang A, Moon BS, Mann I, Harris FW, et al. Macromolecules 1999;32:4784.
[24] Zhu L, Chen Y, Zhang A, Calhoun BH, Chun M, Quirk RP, et al. Phys Rev B 1999;60:10022.
[25] Zhu L, Cheng SZD, Calhoun BH, Ge Q, Quirk RP, Thomas EL, et al. J Am Chem Soc 2000;122:5957.
[26] Hong S, MacKnight WL, Russell TP, Gido SP. Macromolecules 2001; 34:2876.
[27] Hong S, Yang L, MacKnight WL, Gido SP. Macromolecules 2001;34: 7009.
[28] Chen HL, Hsiao SC, Lin TL, Yamauchi K, Hasegawa H, Hashimoto T. Macromolecules 2001;34:671.
[29] Chen HL, Wu JC, Lin TL, Lin JS. Macromolecules 2001;34:6936.
[30] Huang YH, Yang CH, Chen HL, Chiu FC, Lin TL, Liou W. Macromolecules 2004;37:486.
[31] Reiter G, Castelein G, Hoerner P, Riess G, Blumen A, Sommer JU. Phys Rev Lett 1999;83:3844.
[32] Reiter G, Castelein G, Sommer JU, Rottele A, Thurn-Albrecht T. Phys Rev Lett 2001;87:226101.
[33] Bates FS, Fredrickson GH. Annu Rev Phys Chem 1990;41:525.
[34] DiMarzio EA, Guttman CM, Hoffman JD. Macromolecules 1980;13: 1194.
[35] Ye C, Zhang HL, Huang Y, Chen EQ, Lu Y, Shen D, et al. Macromolecules 2004;37:7188.
[36] Jankova K, Chen X, Kops J, Batsberg W. Macromolecules 1998;31: 538.
[37] Zhang D, Liu YX, Wan XH, Zhou QF. Macromolecules 1999;32: 5183.
[38] Zhang H, Yu Z, Wan X, Zhou Q, Woo EM. Polymer 2002;43:2357.
[39] Takahashi Y, Tadokoro H. Macromolecules 1973;6:672.
[40] Chen WY, Li CY, Zheng JX, Huang P, Zhu L, Ge Q. Macromolecules 2004;37:5292.
[41] Wunderlich B. Macromolecular physics, crystal structure, morphology, and defects. vol. 1. New York: Academic Press; 1973.
[42] Point JJ, Damman P, Janimak JJ. Polymer 1993;34:3771.
[43] Marentette JM, Brown GR. Polymer 1998;39:1405.
[44] Chen EQ. PhD Dissertation, Department of Polymer Science, The University of Akron; 1998.
[45] Huang Y, Liu XB, Zhang HL Zhu DS, Sun YJ, Yan SK et al. Submitted.
[46] Hu WB, Frenkel D, Mathot VBF. Macromolecules 2002;35:7172.
[47] Cheng SZD, Chen J, Janimak JJ. Polymer 1990;31:1018.
[48] Hoffman JD, Davis GT, Lauritzen Jr JI. In: Hannay NB, editor. Treatise on solid state chemistry, vol. 3, 1976. p. 497–614.
[49] Hoffman JD, Miller R. Polymer 1997;38:3151.
[50] Schonherr H, Frank CW. Macromolecules 2003;36:1199.